25

Microscopic Theory of Bose-Einstein Condensation of Magnons at Room Temperature

Hayder Salman
School of Mathematics, University of East Anglia Norwich, UK

Natalia G. Berloff
Skolkovo Institute of Science and Technology, Russian Federation
DAMTP, Centre for Mathematical Sciences, Cambridge, UK

Sergej O Demokritov
Institute for Applied Physics and Center for Nonlinear Science,
University of Muenster, Germany;
Institute of Metal Physics, Ural Division of RAS, Yekaterinburg, Russia

A quantised spin wave – magnon – in magnetic films can undergo Bose-Einstein condensation into two energetically degenerate lowest-energy quantum states with non-zero wave vectors $\pm \boldsymbol{k}_{BEC}$. This corresponds to two interfering condensates forming spontaneously in momentum space. Brillouin Light Scattering studies for a microwave-pumped film with sub-micrometer spatial resolution experimentally confirm the existence of the two wave-functions and show that their interference results in a non-uniform ground state of the condensate with the density oscillating in space. Moreover, fork dislocations in the density fringes provide direct experimental evidence for the formation of pinned half quantum vortices in the magnon condensate. The measured amplitude of the density oscillation implies the formation of a non-symmetric state that corresponds to non equal occupation of two energy minima. We discuss the experimental findings and consider the theory of magnon condensates which includes, to leading order, the contribution from the non-condensed magnons. The effect of the non-condensed magnon cloud is to increase the contrast of the asymmetric state and to bring about the experimental measurements.

25.1 Introduction

Magnons are quasiparticles corresponding to quantized spin waves that describe the collective motion of spins [1]. In recent years, it has become pos-

sible to realize a BEC of magnons in two remarkably different systems: in superfluid phases of an isotope of helium – Helium-3 at ultra-low temperatures [3, 4] and in ferrimagnetic insulators [5, 6, 7, 8]. In the normal, non-condensed state, these magnetic materials exhibit a magnetically ordered state with a gas of magnons whose phases are not correlated. However, once condensation occurs, spins develop phase coherence resulting in a common global frequency and phase of precession. At room temperature, ferrimagnetic insulators, such as yttrium-iron garnet (YIG) films, together with a combination of an in-plane magnetic field and microwave radiation are required for the magnon condensation [5, 6, 7, 8]. Therefore, in analogy with exciton-polariton condensates, this provides yet another example of a BEC of quasiparticle excitations in a solid state system.

25.2 Experimental realisation of a Bose-Einstein condensate of magnons in an epitaxial YIG-film

A room-temperature Bose-Einstein condensate of magnons was created in an epitaxial YIG-film using an experimental setup shown in Fig. 25.1a, which, in general, is similar to that used in our previous studies [5, 6]. Given that magnons are quasiparticle excitations, their number is not conserved and, therefore, the chemical potential is zero. To reach the critical value of the chemical potential, necessary for BEC formation, we inject additional magnons using microwave parametric pumping. After thermalisation, the injected magnons gather in two energetically degenerate minima of the energy spectrum located at $\pm\boldsymbol{k}_{\mathrm{BEC}} = \pm\mathbf{Q} = (0, \pm Q)$. In fact, the energy spectrum is anisotropic and arises from the combined effects of the long-range magnetic dipole interactions that break the isotropy of the spectrum and the short range exchange interactions. The additional effects of pumping together with dissipation, caused by the spin–lattice interactions, results in a system that is driven out of equilibrium. However, for magnons, a quasi-equilibrium state with a non-zero chemical potential can be realised because the magnon lifetimes, set by the spin–lattice relaxation times (~ 1 ms), are long compared to the magnon–magnon thermalisation time (~ 100 ns). Therefore, in contrast to BECs of other quasiparticle excitations such as exciton-polariton condensates, a magnon BEC can be considered to be in quasi-equilibrium. This situation implies that an equilibrium statistical mechanical approach is expected to provide a reasonably accurate description of this system.

Condensation into two nonzero values of the wave vector $\pm\boldsymbol{k}_{\mathrm{BEC}}$ leads to

an anisotropy of the condensate ground state and coexistence of two spatially overlapping condensates with the order parameters $\psi_{\pm Q}$. In [9], Brilloun Light Scattering (BLS) was used to measure the total magnon density $|\psi|^2$ where $\psi = \psi_Q \exp[iQz] + \psi_{-Q} \exp[-iQz]$, and we have assumed that the in-plane magnetic field is along the z-direction. Therefore, by scanning the probing laser spot in the two lateral directions and recording the BLS intensity, spatial distribution of the condensate density can be visualised. Figure 25.1c shows the results of a two-dimensional mapping of the condensate density across an $8 \times 5 \mu\text{m}^2$ area of the YIG film adjacent to the pumping resonator, within which the field created by the resonator can be considered as being approximately uniform. The mapping was performed by repetitive scanning of the spatial area followed by the averaging of the recorded data to improve the signal-to-noise ratio. The map clearly demonstrates a periodic pattern along the direction of the static magnetic field created because of interference of the two components of the magnon condensate. The spatial period of the pattern $0.9 \pm 0.1 \mu\text{m}$ obtained from a two-dimensional Fourier transform of the recorded map (Fig. 25.1d), agrees well with the period $0.92 \mu\text{m}$ calculated based on the known value $k_{\text{BEC}} = 3.4 \times 10^4 \text{cm}^{-1}$. It is important to recognise that in the absence of the phase-locking between the two condensates, the evolution of the phase difference between the two condensate order parameters would lead to changes in the spatial positions of the maxima and minima and would not show in the time averaged results. The observed spatial modulation in the BLS intensity is therefore clear evidence of the locking of the coherent phases between the two components that must be explained by any successful theory of magnon condensation.

The interference experiments not only provide direct evidence of the spatial coherence of the magnon condensate in YIG films, but also indicate that a strong asymmetry exists in the number density of the two condensates. To see this, we recall that the average BLS intensity is proportional to the total density of the condensate. It grows with pumping power, increasing from the BEC-transition threshold of 6 mW to 100 mW and then saturates due to the reduction of the parametric pumping efficiency as shown in Fig. 25.2. At the same time, the modulation depth increases quickly above the threshold and then stays nearly constant. As shown in the figure, the measured contrast defined as

$$\beta = \frac{|\psi|^2_{\text{max}} - |\psi|^2_{\text{min}}}{|\psi|^2_{\text{max}} + |\psi|^2_{\text{min}}} \tag{25.1}$$

is seen to be equal to $\beta = 0.035$. However, by accounting for the spatial

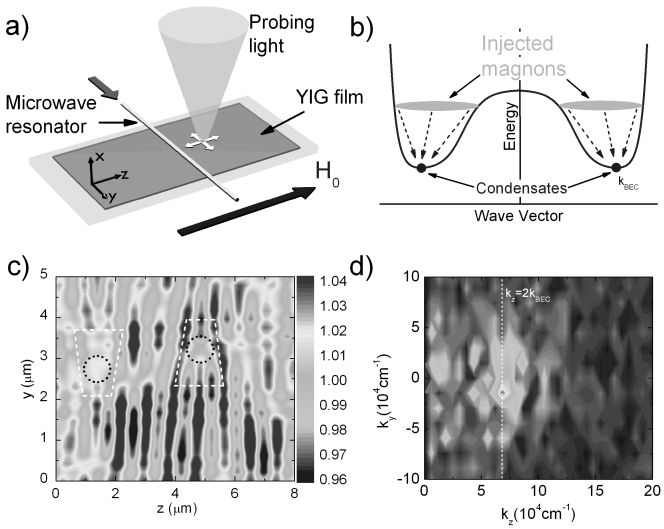

Figure 25.1 Schematic of the experiment and results of two-dimensional imaging of the condensate density. (a) Experimental setup. Magnons are injected into the YIG film using a microwave resonator. After thermalisation they create a Bose-Einstein condensate, which is imaged by scanning the probing laser light in two lateral directions. (b) Qualitative picture of the magnon spectrum in a ferromagnetic film. Injected magnons thermalise and create two Bose-Einstein condensates at two degenerate spectral minima with non-zero wave vectors $\pm \boldsymbol{k}_{\mathrm{BEC}}$. (c) Measured two-dimensional spatial map of the BLS intensity proportional to the condensate density, obtained at the maximum used pumping power. Dashed circles show the positions of topological defects in the standing-wave pattern corresponding to a non-uniform ground state of the condensate. (d) Two-dimensional Fourier transform of the measured spatial map. Dashed line marks the value of the wave vector equal to $2k_{\mathrm{BEC}}$. The spread of the spectral peak and its slight displacement with respect to $k_y = 0$ are caused by the presence of topological defects resulting in a non-zero slope of the real-space stripe structure, as well as by slight misalignment between the static magnetic field and the scanning axis. Reprinted with permission from Nowik-Boltyk, P. *et al.* (2013), Spatially non-uniform ground state and quantized vortices in a two-component Bose-Einstein condensate of magnons, Scientific Reports **2**, 482 [9]. Copyright (2013) by the Nature Publishing Group.

resolution of the measuring probe, we estimate the actual contrast in the experiment to be $\beta = 0.12 - 0.15$.

The above observations provide direct evidence for the coexistence of a two component BEC of magnons which are interlocked through their phase coherence. The production of interference fringes associated with the densities of the two components also allows us to identify vortices in our magnon

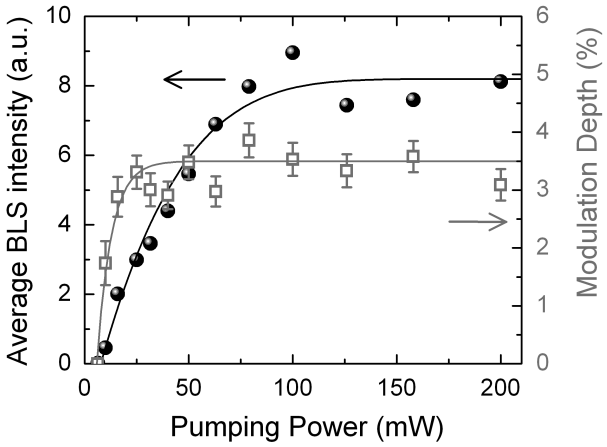

Figure 25.2 Effect of the pumping power on the condensate density and on the amplitude of the standing wave. Filled symbols show the average BLS intensity proportional to the total density of the condensate. Open symbols show the relative depth of the spatial modulation of the BLS intensity, which characterizes the strength of the phase locking between the condensate components. The data were obtained from one-dimensional scans parallel to the direction of the static field. Reprinted with permission from Nowik-Boltyk, P. *et al.* (2013), Spatially non-uniform ground state and quantized vortices in a two-component Bose-Einstein condensate of magnons, Scientific Reports **2**, 482 [9]. Copyright (2013) by the Nature Publishing Group.

condensate. A clear signature of the formation of vortices is the appearance of a fork-like dislocation in the interference pattern as seen in Fig. 25.1c. These quantised vortices, which spontaneously appear during the condensation process [10], are pinned by the crystalline defects present in the sample. The number of prongs present in the interference fringes leads us to conclude that the vortices we observe are analogous to half quantum vortices (fractional vortices) which have also been observed in exciton-polariton condensates [18]. To illustrate this, we present in Fig. 25.3 three density fields produced by assuming a condensate wavefunction of the form $\psi = \psi_Q \exp[iQz] + \psi_{-Q} \exp[-iQz]$. We prescribe the background values of $|\psi_Q|^2 = n_{+Q}$ and $|\psi_{-Q}|^2 = n_{-Q}$ to reproduce the measured contrast of 15% but in each case[1] we make different assumptions on what vortices exist

[1] (a) $\psi_Q = \sqrt{n_{+Q}}(z+iy)/\sqrt{z^2+y^2+n_{+Q}^{-1}}$, $\psi_{-Q} = \sqrt{n_{-Q}}(z-iy)/\sqrt{z^2+y^2+n_{-Q}^{-1}}$;
(b) $\psi_Q = \sqrt{n_{+Q}}(z+iy)/\sqrt{z^2+y^2+n_{+Q}^{-1}}$, $\psi_{-Q} = \sqrt{n_{-Q}}$;
(c) $\psi_Q = \sqrt{n_{+Q}}(z+iy)/\sqrt{z^2+y^2+n_{+Q}^{-1}}$, $\psi_{-Q} = \sqrt{n_{-Q}}(z+iy)/\sqrt{z^2+y^2+n_{-Q}^{-1}}$,
with $n_{-Q} = 0.15 n_{+Q}$.

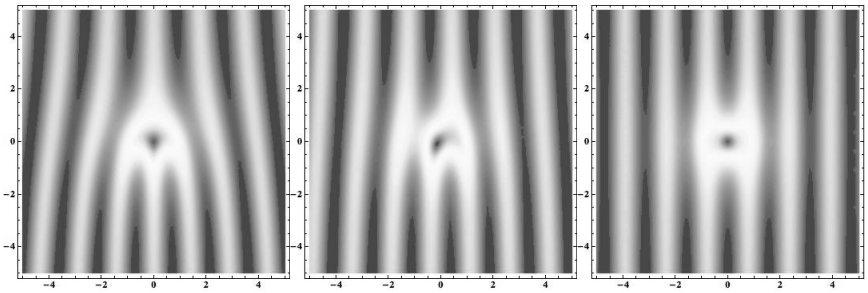

Figure 25.3 Density field in the presence of vortices: (a) Vortex in first component and antivortex in component two; (b) vortex in component one only; (c) vortices in both components.

in each component. As can be seen, assuming a single vortex in one component produces best agreement with the observed density fringes in the experiments.

25.3 A theoretical description of the Bose-Einstein condensation of magnons

Recently, a description of BEC in microwave-pumped YIG films was proposed [11] that accounted for the 4th order interactions and magnon-non-conserving terms of the dipolar interactions. The theory was able to explain the appearance of asymmetric states but the contrast obtained was much smaller ($\sim 1\%$) than the actual experimentally observed ($\sim 12 - 15\%$). In fact, the value of 3.5% presented in Fig. (25.2) does not account for the spatial resolution of the probing laser light which is about $0.55\mu m$ and therefore of the same order as the wavelength $0.92\mu m$ associated with the interference pattern created by the two condensates. This results in significant averaging over the oscillation and leads to an underestimation of the contrast. It can be shown that the experimental measurement needs to be multiplied by a correction factor of 3.43 producing this relatively higher value of contrast. This discrepancy has been remedied in [12] by including the effect of the non-condensed thermal cloud of magnons on the condensate within a Hartree-Fock approximation. It turns out that, apart from depleting the condensate, the thermally excited non-condensed magnons increase the contrast of the asymmetric state and bring about the experimental measurements.

To adopt a microscopic description of the problem, we recognise that on energy scales relevant to the experiments, only the lowest ferromagnetic magnon band is important. The magnetic properties of YIG can then be

described in terms of a quantum Heisenberg ferromagnet on a cubic lattice given by the Hamiltonian

$$\hat{\mathcal{H}} = -g\mu_B H_0 \sum_j \hat{S}_j^z - J \sum_{j,\boldsymbol{\delta}} \hat{\mathbf{S}}_j \cdot \hat{\mathbf{S}}_{j+\boldsymbol{\delta}} + U_d \sum_{i \neq j} \frac{\hat{\mathbf{S}}_i \cdot \hat{\mathbf{S}}_j - 3(\hat{\mathbf{S}}_i \cdot \mathbf{n}_{ij})(\hat{\mathbf{S}}_i \cdot \mathbf{n}_{ij})}{|r_{ij}|^3},$$

for the spin operators $\hat{\mathbf{S}}_j = (\hat{S}_j^x, \hat{S}_j^y, \hat{S}_j^z)$. The various terms account for the Zeeman energy, the exchange interactions, and the dipolar interactions, respectively. Here, μ_B is the magnetic moment (Bohr magneton), $g = 2$ is the Landé factor, H_0 is the externally applied magnetic field, and J and U_d are the exchange and dipolar interaction constants, respectively . The sums i, j are taken over lattice sites at positions $\mathbf{r}_i$, $\boldsymbol{\delta}$ represents a vector to one of the nearest neighbours of i, $\mathbf{r}_{ij} = (\mathbf{r}_i - \mathbf{r}_j)/a_0$, $\mathbf{n}_{ij} = \mathbf{r}_{ij}/|\mathbf{r}_{ij}|$, and $a_0 = 12.376\mathring{A}$ is the lattice constant.

Since we are interested in describing spin deviations from the direction of the in-plane externally applied magnetic field, we will consider the action of spin operators on spin states $\left|s_j^z\right\rangle$ where s_j^z denotes the z-quantum number on site j. The total spin operator at j then satisfies $\hat{\mathbf{S}}_j^2 \left|s_j^z\right\rangle = (\hat{S}_j^{x^2} + \hat{S}_j^{y^2} + \hat{S}_j^{z2}) \left|s_j^z\right\rangle = S(S+1) \left|s_j^z\right\rangle$, where S is the effective spin. This means that we can effectively describe the action of $\hat{S}_j^z$ in terms of the other two components of spin at j. We will therefore recast the Hamiltonian into a form that directly incorporates this constraint by eliminating the spin operator $\hat{S}_j^z$. The remaining operators are then encoded into spin raising and lowering operators defined as

$$\hat{S}_j^+ = \hat{S}_j^x + i\hat{S}_j^y, \qquad \hat{S}_j^+ = \hat{S}_j^x - i\hat{S}_j^y. \tag{25.2}$$

We can now relate these spin operators to creation and annihilation bosonic operators $\hat{a}_j^\dagger$ and $\hat{a}_j$ that act on the occupation number basis of spin deviations at site j. This is given by the Holstein-Primakoff transformation [14]

$$\hat{S}_j^+ = \sqrt{2S}\left(1 - \frac{\hat{a}_j^\dagger \hat{a}_j}{2S}\right)^{1/2} \hat{a}_j, \qquad \hat{S}_j^- = \sqrt{2S}\hat{a}_j^\dagger \left(1 - \frac{\hat{a}_j^\dagger \hat{a}_j}{2S}\right)^{1/2} \tag{25.3}$$

The bosonic operators can be expressed in terms of normal modes such that,

$$\hat{a}_j = \sum_{\mathbf{k}} \hat{a}_{\boldsymbol{k}}(x_j) e^{i\mathbf{k}\cdot\mathbf{r}}, \qquad \hat{a}_j^\dagger = \sum_{\mathbf{k}} \hat{a}_{\boldsymbol{k}}^\dagger(x_j) e^{i\mathbf{k}\cdot\mathbf{r}}, \tag{25.4}$$

where $\mathbf{r} = (y, z)$ and $\boldsymbol{k} = (k_y, k_z)$. Given that the thickness of the film is much smaller than the lateral dimensions, we have performed only a partial Fourier summation over the wavenumbers lying within the (y, z) plane of

the film. In contrast, we have retained the spatial dependence on the x-coordinate that is aligned along the thickness of the film. This is because the transverse modes along x are expected to be sensitive to the effect of the boundaries and can not be approximated using plane waves. However, if we focus on formulating an effective theory for quantities averaged over the thickness of the film, we can drop the dependence on the x spatial coordinate. This results in the so-called uniform mode approximation. To proceed, we now assume that the number of spin deviations in the system is small and exploit the fact that the effective spin $S \simeq 14.2$ is quite large to perform an expansion in powers of $1/S$. Hence, by adopting the uniform mode approximation [13] together with a Holstein-Primakoff transformation [14], our Hamiltonian can be expanded up to fourth order terms in $\hat{a}_{\boldsymbol{k}}$ and $\hat{a}^{\dagger}_{\boldsymbol{k}}$ which can be written as

$$\hat{\mathcal{H}} = \hat{\mathcal{H}}_0 + \hat{\mathcal{H}}_2 + \hat{\mathcal{H}}_4 + \cdots$$

where the index of the corresponding part of the Hamiltonian corresponds to the order of the interactions. The quadratic terms given by $\hat{\mathcal{H}}_2$ takes the form

$$\hat{\mathcal{H}}_2 = \hbar \sum_{\mathbf{k}} \left(A_{\boldsymbol{k}} \hat{a}^{\dagger}_{\boldsymbol{k}} \hat{a}_{\boldsymbol{k}} + \frac{1}{2} B_{\boldsymbol{k}} \hat{a}_{\boldsymbol{k}} \hat{a}_{-\boldsymbol{k}} + \frac{1}{2} B^{*}_{\boldsymbol{k}} \hat{a}^{\dagger}_{\boldsymbol{k}} \hat{a}^{\dagger}_{-\boldsymbol{k}} \right), \tag{25.5}$$

where

$$\begin{aligned} A_{\boldsymbol{k}} &= \gamma H_0 + \mathcal{D}k^2 + \gamma 2\pi M (1 - F_k) \sin^2\theta + \gamma 2\pi M F_k, \\ B_{\boldsymbol{k}} &= \gamma 2\pi M (1 - F_k) \sin^2\theta - \gamma 2\pi M F_k. \end{aligned} \tag{25.6}$$

Here, $F_k = \big(1 - \exp(-|kd|)\big)/|kd|$, d is the film thickness, $k^2 = k_y^2 + k_z^2$, θ is the angle between the wavevector $\boldsymbol{k}$ and the in-plane applied magnetic field, $M = 0.14\text{kG}$ is the magnetisation, $\gamma = 12\mu eV/kOe$ is the gyromagnetic ratio, and $\mathcal{D} = 0.24eV\text{Å}^2$ is the coefficient of the exchange interactions [11]. These quadratic terms can be diagonalized by using the Bogoliubov transformation

$$\begin{aligned} &\hat{a}_{\boldsymbol{k}} = u_{\boldsymbol{k}} \hat{c}_{\boldsymbol{k}} + v_{\boldsymbol{k}} \hat{c}^{\dagger}_{-\boldsymbol{k}}, \quad \hat{a}^{\dagger}_{\boldsymbol{k}} = u_{\boldsymbol{k}} \hat{c}^{\dagger}_{\boldsymbol{k}} + v^{*}_{\boldsymbol{k}} \hat{c}_{-\boldsymbol{k}}, \\ &u_{\boldsymbol{k}} = \left(\frac{A_{\boldsymbol{k}} + \hbar\omega_{\boldsymbol{k}}}{2\hbar\omega_{\boldsymbol{k}}} \right)^{1/2}, \quad v_{\boldsymbol{k}} = \operatorname{sgn}(B_k) \left(\frac{A_{\boldsymbol{k}} - \hbar\omega_{\boldsymbol{k}}}{2\hbar\omega_{\boldsymbol{k}}} \right)^{1/2}, \end{aligned} \tag{25.7}$$

where $\operatorname{sgn}(\cdot)$ is the sign function, $|u_{\boldsymbol{k}}|^2 - |v_{\boldsymbol{k}}|^2 = 1$, and the dispersion relation is given by $\omega_{\boldsymbol{k}} = (A_{\boldsymbol{k}}^2 - |B_{\boldsymbol{k}}|^2)^{1/2}$. The quadratic term then reduces to $\hat{\mathcal{H}}_2 = \sum_{\boldsymbol{k}} \hbar\omega_{\boldsymbol{k}} \hat{c}^{\dagger}_{\boldsymbol{k}} \hat{c}_{\boldsymbol{k}}$. Since a magnon BEC consists of two condensates, we write the quadratic term for condensed magnons in terms of the annihilation and

creation operators, $\hat{c}_{\pm\mathbf{Q}}$ and $\hat{c}^{\dagger}_{\pm\mathbf{Q}}$ for two energetically degenerate lowest energy quantum states with non-zero wave vectors $\mathbf{k}_{\mathrm{BEC}} \equiv \pm\mathbf{Q} = (0, \pm Q)$ in 2D momentum space. This gives $\mathcal{H}_2 = \hbar\omega_{\mathbf{Q}}\big(\hat{c}^{\dagger}_{\mathbf{Q}}\hat{c}_{\mathbf{Q}} + \hat{c}^{\dagger}_{-\mathbf{Q}}\hat{c}_{-\mathbf{Q}}\big)$. The next order terms corresponding to $\mathcal{H}_4$ are given by

$$\begin{aligned}\hat{\mathcal{H}}_4 = {} & A\left[\hat{c}^{\dagger}_{\mathbf{Q}}\hat{c}^{\dagger}_{\mathbf{Q}}\hat{c}_{\mathbf{Q}}\hat{c}_{\mathbf{Q}} + \hat{c}^{\dagger}_{-\mathbf{Q}}\hat{c}^{\dagger}_{-\mathbf{Q}}\hat{c}_{-\mathbf{Q}}\hat{c}_{-\mathbf{Q}}\right] + 2B\hat{c}^{\dagger}_{\mathbf{Q}}\hat{c}^{\dagger}_{-\mathbf{Q}}\hat{c}_{-\mathbf{Q}}\hat{c}_{\mathbf{Q}} \\ & + C\left[\hat{c}^{\dagger}_{\mathbf{Q}}\hat{c}_{\mathbf{Q}}\hat{c}_{\mathbf{Q}}\hat{c}_{-\mathbf{Q}} + \hat{c}^{\dagger}_{-\mathbf{Q}}\hat{c}_{-\mathbf{Q}}\hat{c}_{-\mathbf{Q}}\hat{c}_{\mathbf{Q}} + \mathrm{h.c}\right] + D\left[\hat{c}_{\mathbf{Q}}\hat{c}_{\mathbf{Q}}\hat{c}_{-\mathbf{Q}}\hat{c}_{-\mathbf{Q}} + \mathrm{h.c}\right],\end{aligned} \tag{25.8}$$

where h.c denotes the hermitian conjugate.

The first two terms conserve the number of magnons and give rise to self and mutual interaction of the condensates and were obtained in [15], the third term was introduced in [11] and the fourth term in [12]. The last two terms do not conserve the number of magnons and lead to two condensates locking their total phases. The expressions for the coefficients of Eq. (25.9) are

$$\begin{aligned}A &= -\frac{\hbar\omega_M}{4SN}\Big[(\alpha_1-\alpha_3)F_Q - 2\alpha_2(1-F_{2Q})\Big] - \frac{\mathcal{D}Q^2}{2SN}(\alpha_1 - 4\alpha_2), \\ B &= \frac{\hbar\omega_M}{2SN}\Big[(\alpha_1-\alpha_2)(1-F_{2Q}) - (\alpha_1-\alpha_3)F_Q\Big] + \frac{\mathcal{D}Q^2}{SN}(\alpha_1 - 2\alpha_2), \\ C &= \frac{\hbar\omega_M}{8SN}\left[(3\alpha_1+3\alpha_2-4\alpha_3)F_Q + \frac{8}{3}\alpha_3(1-F_{2Q})\right] + \frac{\mathcal{D}Q^2}{SN}\frac{\alpha_3}{3}, \\ D &= \frac{\hbar\omega_M}{4SN}\Big[(\alpha_3-3\alpha_2)F_Q + 2\alpha_2(1-F_{2Q})\Big] + \frac{\mathcal{D}Q^2}{2SN}\alpha_2,\end{aligned} \tag{25.9}$$

where $\hbar\omega_M = 4\pi M\gamma$, $\alpha_1 = u_Q^4 + 4u_Q^2v_Q^2 + v_Q^4$, $\alpha_2 = 2u_Q^2v_Q^2$, and $\alpha_3 = 3u_Qv_Q(u_Q^2+v_Q^2)$. Expressions for A and B were obtained in [15], C (correcting the coefficients in front of α_2 and α_3 [12]) was presented in [11] and D in [12].

We now adopt a classical fields approximation and replace operators with complex numbers. Furthermore, we use the Madelung transformation for $c_{\pm\mathbf{Q}} = \sqrt{N_{\pm Q}}\exp[i\phi_{\pm}]$, and introduce the total number of condensed magnons $N_c = N_Q + N_{-Q}$, the occupation imbalance given by $\delta = N_Q - N_{-Q}$, and the total phase $\Phi = \phi_+ + \phi_-$ to obtain

$$\mathcal{H}_4 = \frac{1}{2}N_c^2\Big[(A+B) - (B + D\cos 2\Phi - A)(\delta/N_c)^2 + 2C\cos\Phi\sqrt{1-(\delta/N_c)^2}\Big]. \tag{25.10}$$

The total number of condensed magnons N_c is set by a balance established between pumping and relaxation that we will not model explicitly. We will, therefore, prescribe N_c based on the experimentally estimated values reported in [5, 6]. We then proceed to calculate the ground state by

minimising the total energy of the system subject to fixed N_c. In this case, the minimum energy is determined by minimising the interaction term given by Eq. (25.10) with respect to δ and Φ. Differentiating (25.10) with respect to Φ and δ gives the fixed points (a) $\Phi = 0, \delta = 0$, (b) $\Phi = \pi, \delta = 0$, (c) $\Phi = 0, (\delta/N_c)^2 = 1 - C^2/(B+D-A)^2$, (d) $\Phi = \pi, (\delta/N_c)^2 = 1 - C^2/(B+D-A)^2$ or (e) $\Phi = \cos^{-1}(-C/2D), \delta = 0$. We discard (e) in the view of the smallness of D in comparison with $|C|$. $\mathcal{H}_4$ is minimised for $\Phi = \pi$ if $C > 0$ and for $\Phi = 0$ if $C < 0$. The minima are determined by the sign of the parameter $\Delta = A - B + |C| - D$. When $\Delta > 0$, $\delta = 0$, which gives rise to the symmetric case $N_Q = N_{-Q}$. When $\Delta < 0$, $\delta/N_c = 1 - C^2/(B + D - A)^2$ corresponds to an asymmetric case.

Substituting the parameters into Eqs. (25.9), we find $A = -0.1685$ mK/N, $B = 8.3395$ mk/N, $C = -0.0138$ mK/N, $D = -0.0017$ mK/N, so that $\Delta < 0$. This gives an asymmetric state with the contrast $\beta = 2\sqrt{N_Q N_{-Q}}/N_c$ of the order of 1%. This is in disagreement with the experiment of [9], where the contrast is around 12–15% once corrections for the resolution of the probing laser light are taken into account. This discrepancy can be explained by accounting for the effect induced by the presence of the thermal cloud of non-condensed magnons that has been neglected in our discussion thus far in deriving the Hamiltonian of the system. By including the effect of the thermal cloud within a Hartree-Fock approximation, we find that the main effect on the condensate is to renormalise the coefficient C to $\tilde{C}$ such that

$$\widetilde{C} = C + \frac{E}{N_c}, \tag{25.11}$$

where E is given by

$$\begin{aligned} E = \frac{1}{2} \Bigg\{ & -{\sum_{\mathbf{k}}}' (D_k/2 + f_{1,k})/N \left[8(u_Q^2 + v_Q^2) u_k v_k \right] \\ & -(D_Q/2 + f_{1,Q})/N \left[{\sum_{\mathbf{k}}}' 16 u_Q v_Q (u_k^2 + v_k^2) + {\sum_{\mathbf{k}}}' 8(u_Q^2 + v_Q^2) u_k v_k \right] \\ & - {\sum_{\mathbf{k}}}' (f_{2,k} + 3f_{2,Q})/N \left[4(u_Q^2 + v_Q^2)(u_k^2 + v_k^2) \right] \\ & + {\sum_{\mathbf{k}}}' (D_{k-Q} + f_{3,k-Q} + D_{k+Q} + f_{3,k+Q})/N \left[4(u_Q^2 + v_Q^2) u_k v_k \right] \\ & + (D_0 + f_{3,0})/N {\sum_{\mathbf{k}}}' \left[8 u_Q v_Q (u_k^2 + v_k^2) \right] \Bigg\} \langle c_k^\dagger c_k \rangle, \end{aligned} \tag{25.12}$$

$\sum'$ implies that $\mathbf{k} \neq (0, \pm\mathbf{Q})$, and

$$\begin{aligned} f_1 &= \frac{\hbar\gamma 2\pi M}{S}\left[(1-F_k)\sin^2\theta + F_k\right]/4 \\ f_2 &= \frac{\hbar\gamma 2\pi M}{S}\left[(1-F_k)\sin^2\theta - F_k\right]/4 \\ f_3 &= \frac{\hbar\gamma 2\pi M}{S}(1-F_k)\cos^2\theta \\ D_k &= -J\sum_{\boldsymbol{\delta}} e^{i\mathbf{k}\cdot\boldsymbol{\delta}} \approx \frac{\mathcal{D}k^2}{2S} - 2J. \end{aligned} \tag{25.13}$$

To evaluate E, we must determine the population of the thermal cloud in mode $\boldsymbol{k}$ denoted by $N_k = \langle c_k^\dagger c_k \rangle$. This must be interpreted as the occupation averaged over the sample thickness d since we are only considering in-plane wavenumbers. We can calculate this by summing over all the energy bands in the sample corresponding to the quantisation of the dispersion relation in the direction normal to the plane of the sample to obtain

$$n_{\mathbf{k}}(T,\mu) = \frac{1}{dL_xL_y}\sum_n \frac{1}{e^{(\hbar\epsilon_{\mathbf{k},n}-\mu)/k_{\mathrm{B}}T_{\mathrm{eff}}}-1}. \tag{25.14}$$

In the above, L_x and L_z denote the extent of the sample in the y and z-coordinate directions respectively and the effective temperature can be taken to be room temperature given by $T_{\mathrm{eff}} = 300K$. The above expression requires knowledge of the full energy spectrum in our sample. Here, we have used the form given by [16]. For the experiment of [9], this yields $E/N_c = -1.3043$ mK/N and for $n_c = N_c/V = 3.5\times10^{18}$ cm^{-3} gives $\widetilde{C} = -1.3181$ mK/N. This sets the contrast to the value $\beta = |\widetilde{C}|/|(B+E-A)| = 15.5\%$ which is in a much better agreement with experiments. We note that the value of n_c used here is in good agreement with experimentally quoted values. Moreover, it corresponds to a condensate number density to total number density ratio of 5.7% which is also in reasonable agreement with experiments.

Finally, we comment on the mean field equations for the two component magnon condensate. Starting with the full Hamiltonian of the system, we can now write the Gross-Pitaevskii system of equations describing the collective excitations of the two condensates as

$$i\hbar\frac{\partial\psi_{\pm Q}}{\partial t} = -\frac{\partial\mathcal{H}}{\partial\psi^*_{\pm Q}}. \tag{25.15}$$

In analogy with approximations used in atomic condensates [17], we will assume a static thermal cloud of magnons. The system of equations is then

given by

$$i\hbar\frac{\partial\psi_{\pm Q}}{\partial t} = -\frac{\hbar^2}{2m}\nabla^2\psi_{\pm Q} + 2AV|\psi_{\pm Q}|^2\psi_{\pm Q} + 2BV|\psi_{\mp Q}|^2\psi_{\pm Q} + CV\big[(\psi_{\pm Q}\psi_{\mp Q} + \psi^*_{\pm Q}\psi^*_{\mp Q})\psi_{\pm Q} + (|\psi_{\pm Q}|^2 + |\psi_{\mp Q}|^2)\psi^*_{\mp Q}\big] + 2DV\psi^*_{\pm Q}\psi^{*2}_{\mp Q} + E\psi^*_{\mp Q} + F\psi_{\pm Q}, \tag{25.16}$$

where F is an interaction coefficient that, similarly to E, is a function of the number of non-condensed magnons.

25.4 Conclusions

We have shown that condensation of magnons in ferrimagnetic insulators such as yttrium-iron garnet films exhibit a number of unique features. The condensation can be realized at room temperature and occurs at two nonzero momenta corresponding to the lowest energy states. Consequently, the ground state of the condensate appears as a real-space standing wave of the total condensate density attenable to the BLS measurements. The occupation of the states is asymmetric as indicated by contrast measurements associated with the standing wave pattern. Moreover, in analogy with exciton-polariton condensates [18], a magnon condensate supports the formation of half-quantized vortices between the two components that are pinned at the cristallographic defects. By modelling this two-component condensate, including the effects of noncondensed thermal cloud of magnons, it is possible to quantitatively explain the observed asymmetry of the occupation of the two condensates and predict a phase transition between symmetric and asymmetric states as the film thickness and the applied magnetic field are varied. Future directions will require the development of models to study nonequilibrium phenomena, such as the process of condensate formation of magnons in YIG films.

Acknowledgements: SOD acknowledges the financial support by the Deutsche Forschungsgemeinschaft and by the Russian Ministry of Education and Science in frame of the programme.

References

[1] V.L. Safonov, Nonequilibrium Magnons: Theory, Experiment, and Applications, (2013).

[2] L. Pitaevskii, S. Stringari, Bose-Einstein Condensation, (2003).
[3] G. Volovik, Twenty years of magnon Bose condensation and spin current superfluidity in 3HeB, J. Low Temp. Phys. 153 (2008), p. 266.
[4] Y.M. Bunkov and G.V. Volovik, Magnon Bose Einstein condensation and spin superfluidity, J. Phys.: Condens. Matter 22 (2010), p. 1.
[5] S.O. Demokritov, V.E. Demidov, O. Dzyapko, G.A. Melkov, A.A. Serga, B. Hillebrands, and A.N. Slavin, BoseEinstein condensation of quasi-equilibrium magnons at room temperature under pumping, Nature 443 (2006), pp. 430433.
[6] V.E. Demidov, O. Dzyapko, S.O. Demokritov, G.A. Melkov, and A.N. Slavin, Observation of spontaneous coherence in BoseEinstein condensate of magnons, Phys. Rev. Lett. 100 (2008), 047205.
[7] A.V. Chumak, G.A. Melkov, V.E. Demidov, O. Dzyapko, V.L. Safonov, and S.O. Demokritov, Bose Einstein condensation of magnons under incoherent pumping, Phys. Rev. Lett. 102 (2009), 187205.
[8] O. Dzyapko, V.E. Demidov, M. Buchmeier, T. Stockhoff, G. Schmitz, G.A. Melkov, and S.O. Demokritov, Excitation of two spatially separated BoseEinstein condensates of magnons, Phys. Rev. B 80 (2009), 060401.
[9] P.Nowik-Boltyk et al, Spatially non-uniform ground state and quantized vortices in a two-component Bose-Einstein condensate of magnons, *Scientific Reports*, **2**, 482 (2013).
[10] Berloff, N. G. and Svistunov, B. V. Scenario of strongly nonequilibrated Bose Einstein condensation. Phys. Rev. A 66, 013603 (2002).
[11] F. Li, W.M. Saslow, V.L. Pokrovsky, Phase Diagram for Magnon Condensate in Yttrium Iron Garnet Film, *Scientific Reports*, **3**, 1372 (2013).
[12] H. Salman, N.G. Berloff and S.O. Demokritov, in preparation 2015.
[13] P. Krivosik, C.E. Patton, *Phys. Rev. B*, **82**, 184428 (2010).
[14] T. Holstein, H. Primakoff, *Phys. Rev.*, **58**, 1098 (1940).
[15] I.S. Tupitsyn, et al, Phys. Rev. Lett. **100**, 257202 (2008).
[16] B.A. Kalinikos, A.N. Slavin, *J. Phys. C: Solid State Phys.*, **19**, 7013 (1986).
[17] A. Griffin, T. Nikuni, E. Zaremba, Bose-Condensed Gases at Finite Temperatures, (2009).
[18] K.G. Lagoudakis, T. Ostatnický, A.V. Kavokin, Y.G. Rubo, R. André, B. Deveaud-Plédran, *Science*, **326**, 974 (2009).